Temperature Stabilized Surface Reconstructions at Polar ZnO(0001)

Markus Valtiner,[1] Mira Todorova,[2,*] Guido Grundmeier,[1,3] and Jörg Neugebauer[2]

[1]*Christian Doppler Laboratory for Polymer/Metal Interfaces, Max-Planck-Insitut für Eisenforschung GmbH, Max-Planck-Strasse 1, D-40237 Düsseldorf, Germany*

[2]*Department for Computational Materials Design, Max-Planck-Insitut für Eisenforschung GmbH, Max-Planck-Strasse 1, D-40237 Düsseldorf, Germany*

[3]*Technical and Macromolecular Chemistry, University of Paderborn, Warburger Strasse 100, 33098 Paderborn, Germany*

(Received 7 April 2009; published 7 August 2009)

The atomic structure of the polar ZnO(0001) surfaces in a dry and humid oxygen environment is studied combining diffraction experiments and density-functional theory. Our results indicate that for similar stoichiometries a large number of very different, but energetically almost degenerate reconstructions exist. Thus vibrational entropy, which could be safely neglected for most semiconductor surfaces becomes dominant, giving rise to a hitherto not reported strong dependence of surface phase diagrams on temperature. Based on this insight we are able to consistently describe and explain the experimentally observed surface structures on polar ZnO(0001) surfaces.

DOI: 10.1103/PhysRevLett.103.065502 PACS numbers: 81.65.Mq, 68.43.Bc

The use of ZnO in such diverse technological areas as catalysis, corrosion, adhesion, gas sensing, and micro- or optoelectronic devices has triggered widespread interest in this material [1–5]. Being essential for any of these applications, knowledge of the surface structure and stoichiometry is of particularly high practical interest. Despite numerous experimental and theoretical studies the surface structure of ZnO remains elusive. Various microscopic models stabilizing polar surfaces have been suggested, e.g., creation of metallic surface states, removal of surface atoms, or adsorption of impurity atoms [1–3,6–9]. However, the different mechanisms and structures are controversially discussed. A prominent example is the debate whether a (2×2) or a $(\sqrt{3} \times \sqrt{3})R30°$ reconstruction is more stable [10]. Interestingly, while these structures were intensively discussed in the 1970s, neither has been observed in more recent studies, which mainly reported triangular island structures [7].

ZnO is a wide direct band gap semiconductor which crystallizes in the wurtzite structure. Cleaving a ZnO crystal perpendicular to the c axis results in the formation of the oxygen-terminated $(000\bar{1})$ and the zinc-terminated (0001) polar surfaces. Because of the high density of partially occupied states [each zinc (oxygen) dangling bond is filled with $1/2$ $(3/2)$ electrons] such surfaces are unstable and prone to reconstructions. Indeed, although (0001) ZnO surfaces prepared by sputtering and subsequent annealing cycles in UHV conditions have been shown to give rise to a (1×1) LEED pattern, STM measurements by Dulub *et al.* [7] reveal a morphology characterized by a large number of differently sized triangular pits and islands. It has been suggested that these features are the dominant stable reconstruction in the absence of hydrogen for a wide range of oxygen and hydrogen chemical potentials [7,8] and a consequence of electrostatics which causes a reduction of the Madelung energy upon formation of two dimensional islands [7,8].

In the present Letter results of a detailed experimental and density-functional theory (DFT) study on the morphology of ZnO(0001) polar surfaces in dry and humid oxygen atmosphere are given. Our experimental data show surfaces with (2×2) and $(\sqrt{3} \times \sqrt{3})R30°$ reconstructions, which are consistent with the early observations, but cannot be explained based on the recently derived theoretical surface phase diagrams. Performing density-functional theory calculations for an extensive set of surface structures and including temperature effects due to surface vibrational entropy we construct phase diagrams, which depend on chemical potentials and temperature. Our results for hydrogenated ZnO surfaces show that in contrast to common belief the explicit temperature dependence can dominate, giving rise to surface structures, which are completely absent in the previously studied $T = 0$ K phase diagrams. Based on this insight we are able to address the long standing debate.

All experiments were performed using hydrothermally grown ZnO crystals, obtained from MaTeck GmbH (Jülich, Germany), with the ZnO(0001)-Zn side chemomechanically polished with colloidal silica. The correct orientation of the crystals was confirmed by their chemical etching behavior [3]. To ensure well-defined single crystalline surfaces, the crystals were pretreated by etching in a 3N NaOH solution [2] before annealing. Subsequent annealing procedures were carried out using a setup described elsewhere [2,3]. Oxygen gas with a quality of 4.8 was used for the experiments. All exposures were isothermal with the temperature kept at 950 °C ± 3 °C and ambient pressures for 48 h. The samples were cooled down afterwards to 450 °C within 6 h and kept at this final temperature for another 2 h to ensure thermodynamic equilibrium. Subsequent transfer of the samples from the furnace to the UHV introduction chamber took less than 2 min, ensuring that we measure the ''frozen in'' geometries obtained at the

preparation temperatures. The LEED measurements were performed at close-to-normal electron incidence with emission energies from 20 to 120 eV in an UHV system with a base pressure of 10^{-10} mbar.

For the purpose of this work we used two different settings to anneal the crystals, which lead to the formation of distinct morphologies, as indicated by the LEED patterns exemplarily shown in Fig. 1. A structure with (2×2) periodicity [Fig. 1(a)] is seen at the ZnO(0001) surface annealed in a dry oxygen atmosphere (containing at maximum 2 ppm water). Annealing in a humidified oxygen atmosphere containing water with a partial pressure of 40 mbar leads to the appearance of a structure with a $(\sqrt{3} \times \sqrt{3})R30°$ LEED image [Fig. 1(b)]. Angle resolved XPS-spectroscopy measurements, performed after the sample introduction into the UHV chamber, show no sample contamination and clearly indicate the presence of hydroxide at the surface of samples prepared in humid oxygen atmosphere [2]. AFM experiments on these surfaces show atomically flat several micrometers wide terraces and the absence of triangular pits.

To identify the geometries giving rise to the observed LEED patterns, we performed *ab initio* calculations in combination with atomistic thermodynamics [11,12]. Our first-principles approach is based on density-functional theory in the Perdew-Wang-91 [13] generalized gradient approximation, using the projector augmented wave method [14] as implemented in VASP [15]. With this setup we determined the equilibrium lattice parameters for ZnO to be $a = 3.281$ Å and $c/a = 1.615$, in good agreement with previous experimental [16] and theoretical work [8,17]. For the surface calculations a $(8 \times 8 \times 1)$ Γ-point centered mesh was used to sample the Brillouin zone of the primitive (1×1) surface unit cell, while the energy cutoff chosen for the plane-wave basis set was 550 eV. The surface was modeled using a supercell approach with slab geometries consisting of five double layers of ZnO separated by a vacuum of about 20 Å. Dangling bonds on the oxygen-terminated side of the slab were passivated by pseudo H atoms with a valence of $1/2e^-$, to avoid spurious charge transfer from the back to the top surface of the slab. The upper four double layers of ZnO were allowed to relax, while the remaining layers at the bottom of the slab were kept fixed. Convergence tests show that this choice yields total energies converged to within $10\,\mathrm{meV}/(1 \times 1)$ unit cell.

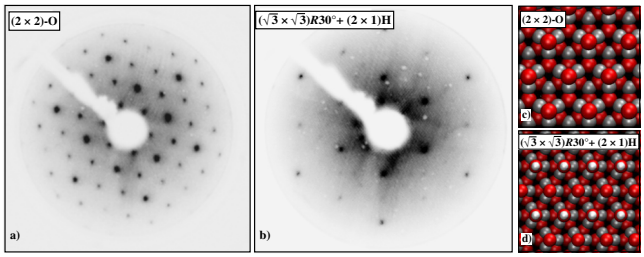

FIG. 1 (color online). LEED images obtained at 63 eV showing the (2×2) periodicity of the surface prepared in clean oxygen atmosphere (a) and the $(\sqrt{3} \times \sqrt{3})R30°$ periodicity of the surface prepared in humid oxygen atmosphere (b). Corresponding stable structures identified by theory are shown in (c) and (d). O atoms: red, Zn atoms: gray, and H atoms: white balls.

Employing different sized surface unit cells we investigated by DFT an extensive set of more than 50 configurations with surface structures including vacancies, adsorbates, and triangular atom arrangements. Based on the computed energies $E^{\sigma}_{\mathrm{tot}}$ [18], with σ labeling the corresponding surface reconstruction, we construct the surface phase diagram employing *atomistic thermodynamics* [11,12]. The key quantity needed to construct such a diagram is the excess Gibbs energy

$$\Delta G_{\sigma} = E^{\sigma}_{\mathrm{tot}} - T\Delta S - \sum_{\alpha} N_{\alpha}\mu_{\alpha} \qquad (1)$$

resulting from the reaction of the surface with atoms in the surrounding (ambient) gas phase. Here, T is the temperature of the surface, ΔS the entropy of the surface atoms, N_{α} the number of surface atoms of species α with corresponding chemical potential μ_{α} of the respective reservoir (e.g., gas phase). The entropic contribution due to temperature driven volume effects is small (<1 meV/atom) and is therefore neglected. Obviously the excess energy $\Delta G_{\sigma}(T, \mu_{\alpha})$ has an explicit temperature dependence due to surface entropy and an implicit T dependence via the chemical potential $\mu_{\alpha} = \mu_{\alpha}(p_{\alpha}, T)$, which is a function of the partial pressure p_{α} and temperature of the gas phase. The implicit T dependence is related to the entropy of the gas phase, which can be under realistic conditions an order of magnitude larger than the entropy of the surface atoms [12]. Thus the dominant temperature effect is attributed to the chemical potential and the excess energy is often approximated by $\Delta G_{\sigma}(T, \mu_{\alpha}(p_{\alpha}, T)) \approx \Delta G_{\sigma}(\mu_{\alpha}(p_{\alpha}, T))$, which provides an easy way to reduce the dimensionality of such phase diagrams [11]. Indeed, previous studies on ZnO surfaces relied on this approximation [8].

In the following we will extend this concept and take the explicit T dependence into account. The thermodynamically stable region of the phase diagram is obtained by considering that ZnO is in thermodynamic equilibrium with the gas phase and that μ_{Zn} and μ_{O} are mutually dependent, which results in an upper (lower) bound for μ_{O} due to the formation of O_2 molecules (Zn bulk). The excess energy can be then expressed as a function of three independent variables, $\Delta G_{\sigma}(T, \mu_{\mathrm{O}}, \mu_{\mathrm{H}})$. An additional constraint is given by $\mu_{\mathrm{O}} + 2\mu_{\mathrm{H}} < \Delta_f H(\mathrm{H_2O}) = -2.59$ eV, since H and O atoms in the gas phase can form H_2O molecules.

Neglecting initially the explicit T dependence we construct the phase diagram shown in Fig. 2(a). An overall good agreement with the previously published phase diagram [8] is found. We attribute minor deviations in the absolute position of phase boundaries to differences in the used parameter setup and rather shallow intersections of the respective phase planes. For low hydrogen chemical

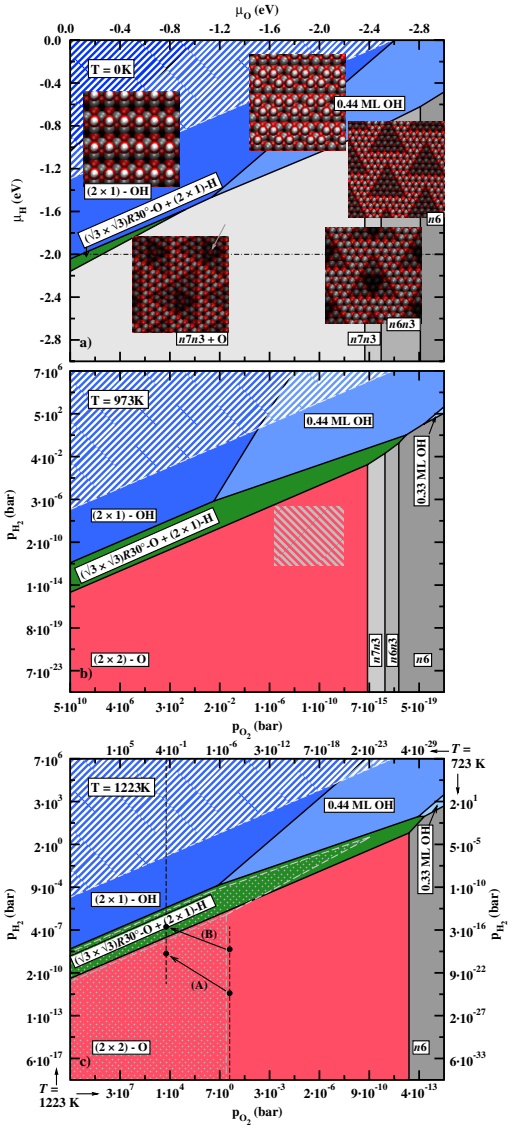

FIG. 2 (color online). Phase diagram for the ZnO(0001)-Zn surface in equilibrium with a humid oxygen atmosphere for different temperatures. Equilibrium conditions under which water would condensate on the surface are indicated by the hashed area (upper left corner). (a) $T = 0$ K. The geometries of the stable surface structures are shown as insets and in Figs. 1(c) and 1(d). The oxygen atom in $n3n7 + \mathrm{O}$ indicated by a gray arrow is absent in $n3n7$ (not shown). The hydrogen chemical potential μ_{H} used to construct Fig. 3 is marked by a dot-dashed black line. (b) $T = 973$ K. The hashed square marks characteristic conditions of the UHV experiments [10] (cf. text). (c) $T = 1223$ K. Dot filled areas depict regions of thermodynamic stability for $(\sqrt{3} \times \sqrt{3})R30°\,\mathrm{O} + (2 \times 1)\mathrm{H}$ and (2×2)-O at $T = 723$ K. Parameters corresponding to our experimental setup (cf. text) are marked by black dots and arrows.

potentials the phase diagram is dominated by triangular reconstructions, while geometries containing H become stable upon increasing μ_{H}. In the oxygen-rich region (i.e., high μ_{O}) we find a novel structure which has not been reported in previous theoretical studies. This structure [Fig. 1(d)] exhibits a $(\sqrt{3} \times \sqrt{3})R30°$ periodicity and features alternating rows of oxygen atoms and hydroxyl groups. It has a $(\sqrt{3} \times \sqrt{3})R30°$-O backbone with H atoms adsorbed on top of these O atoms in a (2×1) arrangement. It contains 1/6 ML OH and 1/6 ML O. At even higher H coverage a hydroxylated ZnO surface, with (2×1)-OH periodicity is favored (inset in Fig. 2). Both structures obey electron counting [19].

While the $(\sqrt{3} \times \sqrt{3})R30°$-O + (2×1)-H phase could account for the observed LEED image with periodicity $(\sqrt{3} \times \sqrt{3})R30°$, we note that none of the phases found in the phase diagram can explain the measured (2×2) LEED pattern. Based on the experimental conditions (e.g., $T = 450\,°\mathrm{C}$, $p_{\mathrm{H_2O}} \approx 10^{-5}$ bar) at which we observe the (2×2) periodic structure, we fix μ_{H} [20] and plot in Fig. 3 the dependence of the Gibbs free energy on μ_{O}. Because of their very similar stoichiometries, a number of lines with very similar slopes, but representing very different geometries are found within a rather narrow window of 20–30 meV. This very narrow energy interval suggest that differences in vibrational entropy of the various surface structures may dominate free energy differences at higher temperatures.

We therefore determine the vibrational frequencies for surface, subsurface, and edge O and Zn atoms, as well as for O and H atoms and OH groups adsorbed at the surface. We calculate the force constant K_i for each of these atoms or groups by displacing them along a set of inequivalent directions and freezing the remaining atoms in the structure at their optimized equilibrium positions. The frequency within the harmonic approximation is then $\omega_i = \sqrt{K_i/M_i}/(2\pi)$, with M_i the mass of the atom or group. The calculated modes are used to evaluate the vibrational contribution to Gibbs' free energy following the procedure described in Refs. [11,12]. Including vibrational entropy renders the phase diagram explicitly temperature dependent, leading to dramatic changes as the temperature is increased [compare Fig. 2(a) with 2(b) and 2(c)]. This change is a consequence of the high vibrational entropy of surface atoms in adatom structures. To

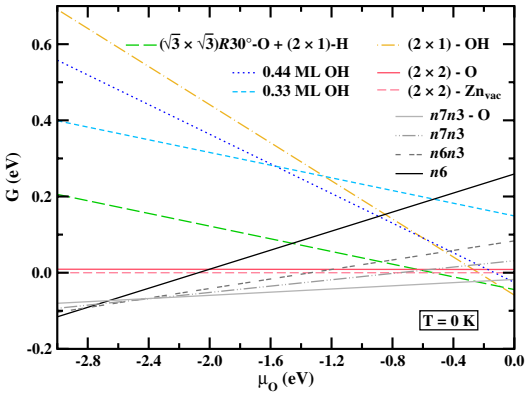

FIG. 3 (color online). Dependence of the Gibbs free energy of formation on the oxygen chemical potential μ_{O} for $\mu_{\mathrm{H}} = -2$ eV (see text).

give an example, at $T = 450\,^{\circ}\mathrm{C}$ entropic contributions lower the energy of the (2×2)-O by 88 meV/atom, while for the triangular $n7n3 + \mathrm{O}$ structure the corresponding stabilization is only 36 meV/atom. Both high temperature phase diagrams shown in Fig. 2 prominently feature a (2×2)-O adlayer structure, with O adsorbed in hollow sites [cf. Fig. 1(c)]. This reconstruction is consistent with the measured LEED pattern. We finally note that the close proximity between oxygen acceptor and zinc donor atoms in this structure minimizes the energy cost for an electron transfer from a zinc to an oxygen dangling bond, making it one of the most obvious stabilization configurations [21] obeying electron counting.

The phase diagram for $T = 973$ K [700 °C, Fig. 2(b)] depicts conditions at which *in situ* UHV-LEED experiments found in the literature of the 1970s [10] have been performed ($T = 973$ K, $10^{-13} < p_{\mathrm{O}_2} < 10^{-6}$ bar, $10^{-12} < p_{\mathrm{H}_2} < 10^{-7}$). We note that part of the marked area lies in close proximity to the border line between the (2×2)-O and $(\sqrt{3} \times \sqrt{3})R30°$-O + (2×1)-H phases, making the observation of either of these structures plausible.

To discuss our experimental conditions we have included in Fig. 2(c) the relevant part of the diagram for $T = 723$ K (450 °C): The temperature driven changes in the phase boundaries are marked by dashed gray lines (dot filled areas). The experimental conditions, which lead to the (2×2) LEED pattern are marked by path A ($T = 1223\ \mathrm{K} \rightarrow 723$ K, $p_{\mathrm{O}_2} = 1$ bar, $p_{\mathrm{H_2O}} = 0.2$ mbar). This path is contained entirely within the thermodynamic stability region of the (2×2)-O structure and thus consistent with the experimental observations. Similarly, path B ($p_{\mathrm{O}_2} = 0.96$ bar, $p_{\mathrm{H_2O}} = 40$ mbar) marks the experimental conditions leading to the $(\sqrt{3} \times \sqrt{3})R30°$ structure. As can be seen the phase diagram [Fig. 2(c)] predicts a transition from (2×2)-O to $(\sqrt{3} \times \sqrt{3})R30°$-O + (2×1)-H, which is indeed observed in experiment.

In summary, we investigated the morphology of the polar ZnO(0001) surface in dry and humid oxygen atmosphere by combining experiment with DFT calculations supplemented by thermodynamic considerations. We demonstrated that the vibrational entropy of the surface plays a decisive role in the competition between various phases to gain thermodynamic stability, which is in contrast to observations for other materials [11] and the common belief that temperature effects are restricted to the T dependence of the gas phase chemical potentials. The, for semiconductors, unexpectedly large impact of surface vibrational entropy on the stabilization of the surface enables us to understand the great diversity of experimentally observed surface geometries. The delicate balance between the various stable geometries is expected to affect all areas of utilization (e.g., sample preparation, catalysis or corrosion, to name but a few) and implies that surface vibrational entropy may have to be included whenever oxide surfaces come into contact with a humid environment.

This work was supported by voestalpine Stahl Linz GmbH, Henkel Surface Technologies as well as the Christian-Doppler Society in Vienna. Computer time at the Paderborn Center for Parallel Computing PC^2 is gratefully acknowledged.

*m.todorova@mpie.de

[1] C. Wöll, Prog. Surf. Sci. **82**, 55 (2007).
[2] M. Valtiner, S. Borodin, and G. Grundmeier, Phys. Chem. Chem. Phys. **9**, 2406 (2007).
[3] M. Valtiner, S. Borodin, and G. Grundmeier, Langmuir **24**, 5350 (2008).
[4] A. Janotti, D. Segev, and C. G. Van de Walle, Phys. Rev. B **74**, 045202 (2006).
[5] J. E. Northrup and J. Neugebauer, Appl. Phys. Lett. **87**, 141914 (2005).
[6] A. Wander *et al.*, Phys. Rev. Lett. **86**, 3811 (2001).
[7] O. Dulub, U. Diebold, and G. Kresse, Phys. Rev. Lett. **90**, 016102 (2003).
[8] G. Kresse, O. Dulub, and U. Diebold, Phys. Rev. B **68**, 245409 (2003).
[9] B. Meyer, Phys. Rev. B **69**, 045416 (2004).
[10] E.g., S. C. Chang and P. Mark, Surf. Sci. **46**, 293 (1974); M. F. Chung and H. E. Farnsworth, *ibid.* **22**, 93 (1970); H. van Hove and R. Leysen, Phys. Status Solidi A **9**, 361 (1972).
[11] J. E. Northrup, R. Di Felice, and J. Neugebauer, Phys. Rev. B **56**, R4325 (1997); Chris G. Van de Walle and J. Neugebauer, Phys. Rev. Lett. **88**, 066103 (2002).
[12] K. Reuter and M. Scheffler, Phys. Rev. B **65**, 035406 (2001); K. Reuter and M. Scheffler, Phys. Rev. Lett. **90**, 046103 (2003).
[13] J. P. Perdew and Y. Wang, Phys. Rev. B **45**, 13 244 (1992).
[14] P. E. Blöchl, Phys. Rev. B **50**, 17 953 (1994).
[15] G. Kresse and J. Furthmuller, Comput. Mater. Sci. **6**, 15 (1996); G. Kresse and J. Furthmuller, Phys. Rev. B **54**, 11 169 (1996).
[16] H. Karzel *et al.*, Phys. Rev. B **53**, 11 425 (1996); S. Desgreniers, Phys. Rev. B **58**, 14 102 (1998).
[17] B. Meyer and D. Marx, Phys. Rev. B **67**, 035403 (2003).
[18] The poor convergence of the clean surface (metallic) reference causes a slow convergence of $E^{\sigma}_{\mathrm{tot}}$ with respect to slab thickness. To eliminate this intrinsic error we use a correction term $\Delta E_{\mathrm{corr}} = E_{\mathrm{surf}}(X) - E_{\mathrm{surf}}(\mathrm{conv})$, where $E_{\mathrm{surf}}(X)$ and $E_{\mathrm{surf}}(\mathrm{conv})$ are the surface energies calculated for a model containing X-ZnO double layers and a slab containing 18-ZnO double layers (converged value). With this approach we determine $E^{\sigma}_{\mathrm{tot}} = [E_{\mathrm{tot}} - E_{\mathrm{tot}}(\mathrm{clean}) - \Delta E_{\mathrm{corr}}]$, where E_{tot} and $E_{\mathrm{tot}}(\mathrm{clean})$ are the DFT energies of the structure under consideration and the ideal clean surface, converged to within 2 meV using just a 5-ZnO double layers thick slab (for which the correction term amounts to 30 meV).
[19] W. A. Harrison, *Electronic Structure and the Properties of Solids* (Dover Publications, Inc., New York, 1989); M. D. Pashley, Phys. Rev. B **40**, 10 481 (1989).
[20] μ_{H} is calculated from $p_{\mathrm{H_2O}}$ by fixing the oxygen chemical potential at the experimental (T, p) conditions, i.e., $\mu_{\mathrm{H}} = \mu_{\mathrm{H_2O}}(T, p) + \Delta_f H(\mathrm{H_2O}) - \mu_{\mathrm{O}}(T, p)$.
[21] D. J. Chadi, Phys. Rev. Lett. **52**, 1911 (1984).